Everything hits at once - how remote rainfall matters for the prediction of the Canadian heat 2021

Annika Oertel[1], Moritz Pickl[1], Julian F. Quinting[1], Seraphine Hauser[1], Jan Lucas Wandel[2], Linus Magnusson[3], Magdalena Balmaseda[4], Frederic Vitart[4], and Christian Michael Grams[1]

[1]Karlsruhe Institute of Technology
[2]Karlsruhe Intitute of Technology
[3]European Centre for Medium-Range Weather Forecasts
[4]ECMWF

November 21, 2022

Abstract

In June 2021, Canada experienced an intense heat wave with unprecedented temperatures and far-reaching socio-economic consequences. Anomalous rainfall in the West Pacific triggers a cascade of weather events across the North Pacific, which build up a high-amplitude ridge over Canada and ultimately lead to the heat wave. We show that the response of the jet stream to diabatically enhanced ascending motion in extratropical cyclones represents a predictability barrier with regard to the heat wave magnitude. Therefore, probabilistic weather forecasts are only able to predict the extremity of the heat wave once the complex cascade of weather events is captured. Our results highlight the key role of the sequence of individual weather events in limiting the predictability of this extreme event. We therefore conclude that it is not sufficient to consider such rare events in isolation but it is essential to account for the whole cascade over different spatio-temporal scales.

Everything hits at once - how remote rainfall matters for the prediction of the Canadian heat 2021

Oertel, A.[1], Pickl, M.[1], Quinting, J.F., Hauser, S.[1], Wandel, J.[1], Magnusson, L.[2], Balmaseda, M.[2], Vitart, F.[2], Grams, C.M.[1]

[1]Institute of Meteorology and Climate Research (IMK-TRO), Karlsruhe Institute of Technology (KIT), Karlsruhe, Germany
[2]European Centre for Medium-Range Weather Forecasts (ECMWF), Reading, United Kingdom

Key Points:

- Intense North American heat wave 2021 is associated with extremely amplified upper-level ridge
- Magnitude of record-high temperatures was not predicted beyond seven days
- Chain of synoptic-scale precipitation events constitutes predictability barrier

Corresponding author: Annika Oertel, `annika.oertel@kit.edu`

Abstract

In June 2021, Canada experienced an intense heat wave with unprecedented temperatures and far-reaching socio-economic consequences. Anomalous rainfall in the West Pacific triggers a cascade of weather events across the North Pacific, which build up a high-amplitude ridge over Canada and ultimately lead to the heat wave. We show that the response of the jet stream to diabatically enhanced ascending motion in extratropical cyclones represents a predictability barrier with regard to the heat wave magnitude. Therefore, probabilistic weather forecasts are only able to predict the extremity of the heat wave once the complex cascade of weather events is captured. Our results highlight the key role of the sequence of individual weather events in limiting the predictability of this extreme event. We therefore conclude that it is not sufficient to consider such rare events in isolation but it is essential to account for the whole cascade over different spatio-temporal scales.

Plain Language Summary

In June 2021, Canada experienced an intense heat wave with unprecedented temperatures and far-reaching socio-economic consequences. We show that the forecast of the extreme temperature anomalies was limited due to a complex sequence of weather events across the Pacific. Thus, state-of-the-art weather forecasts were only able to predict the magnitude of the heat wave once the cascade of weather events was captured in the forecast.

1 Introduction

The heat wave during the end of June 2021 in Western North America was unprecedented. In Lytton, British Columbia, Canada's previous all-time maximum temperature record dating back to 1937 was exceeded on 29 June by 5 K (Philip et al., 2021; Abraham, 2021). Although heat waves are expected to become hotter in a changing climate (Seneviratne et al., 2021) and the probability of record-breaking extremes with temperatures well above previous records will increase (Fischer et al., 2021), early attribution studies suggested that even under consideration of the current state of climate change, the temperatures of this event were extraordinarily unusual (Philip et al., 2021): the 2 m temperature anomaly with respect to the June-July climatological mean from 1979-2019 reached up to 20 K (Fig. 1a). It is well-known that such extratropical heat waves are typically linked to persistent, quasi-stationary, strongly amplified, upper-level ridges that are embedded in extratropical Rossby waves (Teng et al., 2013; Screen & Simmonds, 2014; Hoskins & Woollings, 2015; Petoukhov et al., 2016; Coumou et al., 2018; Kornhuber et al., 2020; Spensberger et al., 2020) and cause anomalous temperatures through air-mass advection, large-scale subsidence, and clear-sky radiation (Pfahl & Wernli, 2012; Bieli et al., 2015; Quinting & Reeder, 2017; Zschenderlein et al., 2019). The heat wave in Western North America also occurred underneath a high-amplitude stationary upper-tropospheric ridge (Fig. 1a) which was colloquially coined as 'heat dome' (Philip et al., 2021; Capuccini & Samenow, 2021). The upper-tropospheric ridge was characterized by a quasi-stationary negative potential vorticity (PV, Hoskins et al. (1985)) anomaly that extended from the northern U.S. into the north-west territories (Fig. 1a, supporting information Fig. S3). Large-scale subsidence underneath this high-amplitude ridge led to the unusual near-surface temperatures (Qian et al., 2022). Moreover, enhanced lower- to mid-tropospheric moisture trapped the long-wave radiation and thus amplified the temperature anomaly further (Mo et al., 2022). The magnitude of the heat wave was not captured by state-of-the-art numerical weather prediction models at forecast lead times beyond approximately seven days (Fig. 1b; see also Lin et al. (2022)). Only at lead times of less than seven days, the extreme temperatures in Western North America were predicted by the ensemble forecasting system of the European Centre of Medium-Range Weather Forecasts (ECMWF, Fig. 1b; Emerton et al. (2022)). The relatively short lead time due to insufficient medium-range forecasts may have hampered possible disaster mitigation efforts, which may require more time than the predictability horizon of the event (White et al., 2017). On 22 June, seven days prior to the peak of the heat wave, the forecasts of temperature near the surface (not shown) and at 850 hPa (T@850hPa), which is in approximately 1.5 km height and characterizes the regional air mass, abruptly improved (Fig. 1b). Subsequent forecasts captured the record-breaking heat anomaly and the corresponding large-scale flow pattern, indicating the existence of a predictability barrier (Sánchez et al., 2020; González-Alemán et al., 2022) on the synoptic time-scale, which hinders successful predictions of the intense heat on the medium-range timescale extending to up to 15 days lead time. Here, we apply an atmospheric dynamics perspective focusing on the critical role of the chain of synoptic events leading to the strong amplification of the upper-level flow and limiting the medium-range predictability of this extreme event.

2 Methodology

Throughout this study, we use a number of different methodological approaches, including the Lagrangian and Eulerian perspectives of diabatically enhanced ascending airstreams, henceforth referred to as warm conveyor belts (WCBs).

We employ a Lagrangian perspective to highlight the remote influence and the role of diabatically enhanced ascending airstreams for the formation of the upper-level ridge. Based on 3-hourly wind fields from the ERA5 reanalysis (Hersbach et al., 2020), 10-day backward trajectories are started on 29 June 00 UTC within the upper-level ridge between 500 and 150 hPa using LAGRANTO (Wernli & Davies, 1997; Sprenger & Wernli, 2015). Specifically, trajectories are initialized within the negative PV anomaly object identified as a vertically-averaged PV anomaly between 500 to 150 hPa with a deviation of at least -0.69 PVU from the 30-day running mean climatology for 1979 to 2019 (Hauser et al., 2022). Only such trajectories that originate from below 800 hPa, i.e., substantially ascend prior to their arrival in the ridge, are considered (Fig. 2a). Subsequently, the remaining trajectories are classified by the location where (West Pacific or East Pacific) and when their main ascent occurs.

To identify processes that influenced the predictability of the heat wave magnitude and that led to the formation of the upper-level ridge over North America, which was unambiguously linked to the temperature extremes (see section 3.1), we make use of operational ensemble forecasts from the European Centre for Medium-Range Weather Forecasts (ECMWF). The considered forecasts are initialized daily at 00 UTC between 14 and 29 June 2021 and have been retrieved on a 1° x 1° grid. The ensemble comprises 50 perturbed members plus one control forecast. Based on the representation of the upper-level ridge over North America, each of the 765 individual forecasts of the medium-range ensemble initialized between 14 and 28 June at 00 UTC is classified into a group of 'good' or 'bad' forecasts (supporting information Fig. S1). This classification is based on the percentile rank of the domain-average root-mean squared error (RMSE) of potential temperature at the 2 PVU isosurface in the upper-level ridge (145°–95° W, 30°–75° N) valid on 29 June 00 UTC, verified against ECMWF's operational high-resolution analysis. Forecasts with the 30% lowest and highest RMSE are grouped into the 'good' and 'bad' category, respectively, with overall 230 individual forecasts in each group. Within these subgroups, imprints of WCBs, are detected by using a novel technique based on convolutional neural networks (ELIAS2.0; Quinting and Grams (2022a); Quinting et al. (2022); Quinting and Grams (2022b)). ELIAS2.0 takes five atmospheric variables as predictors and provides conditional probabilities of occurrence for three different stages of the ascending airstreams as output. These stages are referred to as inflow for air masses being located in the lower troposphere, ascent for air masses in the mid troposphere, and outflow for air masses in the upper troposphere. The conditional probabilities predicted by ELIAS2.0 are converted to two-dimensional binary imprints for each of the three stages.

3 Results

3.1 Heat wave unambiguously linked to upper-level ridge

To emphasize the dominant role of synoptic events in limiting the predictability of the heat wave magnitude, we analyze the evolution of the upper-level flow in the 'good' forecasts and compare them to the 'bad' forecasts, which have the largest discrepancy in the upper-level flow field (section 2). Good forecasts are solely initialized after 22 June while all bad forecasts are initialized before 23 June (see supporting information Fig. S1), emphasizing the presence of the medium-range predictability barrier on 22 June, i.e., after the abrupt improvement in the T@850hPa ensemble forecast (Fig. 1b). The selected 'good' forecasts that adequately represent the position and amplitude of the upper-level ridge also correctly represent the temperature anomaly at 850 hPa (Fig. 1d). In contrast, the 'bad' forecasts with the largest error in the tropopause height also strongly underestimate the temperature where the heat wave occurred (Fig. 1c). For example near Lytton, T@850hPa was underestimated on average by almost 14 K in the bad forecasts. The bad forecasts are characterized by a too zonal flow across the Pacific and a strong underestimation of the extent of the upper-level ridge (Fig. 1c), and thus, of the heat dome. We conclude that the large-scale, far poleward extending upper-level ridge with anomalously high tropopause heights (supporting information Fig. S2) is a prerequisite for the recorded temperature extremes, and that correct predictions of the heat wave magnitude are unambiguously linked to the correct representation of the ridge amplitude.

3.2 High-amplitude ridge influenced by complex chain of synoptic events

The upper-level ridge was continuously fed by air masses originating to a substantial fraction from the lower troposphere over the North Pacific during the 10 days prior to the heat wave (Fig. 2a): 20% of the trajectories originate from below 800 hPa and are heated diabatically. Within 3 days prior to their arrival in the upper-level PV anomaly 18% of all trajectories are heated by more than 2 K, while this fraction increases to 48% if the time span is extended to 7 days (Pfahl et al., 2015; Steinfeld & Pfahl, 2019). Based on 10-day backward trajectories started within the upper-level ridge, we identified individual ascent episodes across the North Pacific. WCB activity took place predominantly in the West and Central to East Pacific on 21–24 June, and later only in the East Pacific on 25–28 June (Fig. 2b). We also identify an early WCB ascent episode prior to 21 June where WCB trajectories ascending in the West Pacific also reach the upper troposphere and contribute to the ridge's air mass.

In the following, we discuss the role of ascending air masses in both regions for the amplification and maintenance of the ridge over Western North America. This will also highlight the challenge for numerical weather prediction models to correctly predict the sequence of many individual synoptic events which eventually formed the high-amplitude upper-level ridge facilitating extreme temperatures.

During the three days prior to the peak of the heat wave, the ascending air masses over the East Pacific (Figs. 3b,c, green contours based on analysis data) are directly fed into the upper-level ridge (Figs. 3b,c, black contour). The most rapidly ascending airstreams reach the ridge on its upstream and poleward flank. Latent heat release within these WCBs importantly contributed to the amplitude of the upper-level ridge (Neal et al., 2022). The collocation of WCB outflow and anomalously high tropopause heights exceeding the 95th percentile of the climatological height (Figs. 3b,c, orange shading and stippling) indeed suggests that also for this event the WCB outflow maintains the quasi-stationary ridge, re-amplifies the pre-existing PV anomaly and finally leads to a poleward extension of the ridge (Fig. 3a,b,c, supporting information Fig. S2 d,e,f). The East Pacific WCB events are triggered through downstream baroclinic development across the North Pacific a few days earlier (Fig. 3a,b). An initially small amplification of the upper-level Rossby wave in the West Pacific (Fig. 3a) and subsequent development of a ridge-trough pattern in the Central Pacific enables cyclogenesis and WCB ascent ahead of the formed trough. The amplification of the Rossby wave in the West Pacific is associated with the ascending air masses between 21–24 June over the West and Central Pacific. On 24 June, the outflow of WCBs over the West Pacific is juxtaposed with the dynamical tropopause (Fig. 3a). Its anomalous height exceeding the 95th percentile of the climatological value in this region indicates the important contribution of the ascending airstreams to the lifting of the tropopause. The exceptionally high tropopause air mass is transported downstream, as indicated by the trajectories (Fig. 2), and represents an important preconditioning for extreme tropopause heights in the ridge over Western North America.

The significant contribution of diabatic processes and WCB outflow to the anomalous tropopause height is confirmed from a climatological perspective (see Supplementary methods in supporting information): during ten days prior to the peak of the heat wave, the WCB activity across the North Pacific was unusually high, particularly for summer conditions (Fig. 4a). In the East Pacific, the WCB outflow frequency locally exceeds the June climatological mean value by a factor of 10 (Fig. 4a). In the West Pacific, the quasi-stationary Meiyu-Baiu front leads to a local maximum of climatological WCB activity (Madonna et al., 2014; Yihui & Chan, 2005; Ninomiya & Shibagaki, 2007) (black contours in Fig. 4a). Prior to the heat wave, however, the WCB activity is shifted northeast, resulting in anomalously high WCB activity in the Western and Central Pacific which exceeds the climatological mean value by a factor of two (Fig. 4a). The anomalous WCB activity in the West Pacific coincides with a strong precipitation anomaly: satellite observations (see Supplementary methods in supporting information) emphasize the above-normal rainfall that occurred in the second half of June near the Meiyu-Baiu-Front (Fig. 4b). In this region, between 19-23 June, substantial precipitation is associated with WCB ascent, whose outflow plays an important role in pre-conditioning the upper-level jet (Fig. 3a). This corroborates the importance of diabatic processes for the outflow and the lifting of the tropopause as a pre-conditioning of the Rossby wave pattern.

3.3 Synoptic-scale processes limit predictability

The above analysis suggests that the complex interplay of synoptic events over the West and East Pacific contributed significantly to the upper-level ridge. In the following, we will highlight the importance of this interplay for the correct prediction of the heat wave by evaluating ECMWF's ensemble forecasts. The analysis of WCB activity in all individual forecasts (see section 2) shows that forecasts which are characterized by large errors in both the upper-level flow and T@850hPa (i.e., the bad forecasts) consistently underestimate WCB ascent and upper-level outflow across the West and East Pacific prior to the event (Fig. 3). Concerning the WCB activity over the East Pacific, the bad forecasts systematically underestimate the WCB activity three days prior to the event (Figs. 3b, c). This results in a mis-representation of the final ridge position and amplitude (Fig. 3d). This underestimation of WCB activity over the East Pacific and the subsequent mis-representation of the upper-level ridge is linked to erroneous WCB outflow in the West Pacific on 24 June (Fig. 3a). This diabatic outflow in the West Pacific amplifies the upper-level Rossby wave pattern and subsequently enables WCB ascent ahead of the developing trough downstream (Fig. 3b). The bad forecasts position WCB outflow and the associated ridge too far to the west (Fig. 3a), and thus miss the correct downstream flow evolution.
To summarize, the mis-representation of WCB outflow in the West Pacific (Fig. 3a) and its interaction with the upper-level jet leads to an underestimation of WCB activity in the East Pacific (Fig. 3b,c), finally resulting in an erroneous position and amplitude of the upper-level ridge (Fig. 3d). The considerable underestimation of the temperature under the ridge by the bad forecasts highlights the relevance of this specific chain of synoptic events

for the occurrence and prediction of such rare temperature extremes.

To address the role of West Pacific precipitation for the predictability barrier for the Western North American heat wave, tailored relaxation experiments were performed (Magnusson, 2017). For that purpose, ensemble re-forecasts were initialized on 19, 20, and 21 June and were drawn towards the truth in the region surrounding the West Pacific precipitation anomaly (see Supplementary methods in supporting information). The correct representation of the atmospheric state in the West Pacific during the intense precipitation events improves the forecast of the heat wave: the upper-level flow across the Pacific is represented more accurately, and in particular, the development of the Central Pacific trough on 27 and 28 June improves (supporting information Fig. S4). The representation of the final ridge position in the relaxation experiments on 29 June is improved, in particular its westward extension and the position of the upstream trough. Nevertheless the poleward extent is still underestimated (supporting information Fig. S4). Accordingly, the temperature is still too low in the relaxation experiments (gray boxes and purple diamonds in Fig. 1b), although the ensemble mean is increased compared to the operational forecasts (supporting information Fig. S4) and the ensemble distribution is shifted closer to the magnitude of the heat wave (Fig. 1b). Thus, the correct representation of the interaction of precipitation with the atmospheric flow in the West Pacific leads to improved, yet imperfect forecasts. For comparison, the same nudging experiments were performed with relaxation in a box shifted further upstream. These experiments, however, did not improve the forecast of the heat wave (supporting information Fig. S5). We conclude that precipitation at the Meiyu-Baiu-Front in the West Pacific prior to the predictability barrier on 22 June and its interaction with the upper-level jet are important for the pre-conditioning of the Rossby wave pattern and set the stage for synoptic processes downstream. The predictability barrier of the heat wave at seven days lead time is thus linked to the mis-representation of West Pacific synoptic conditions. Nevertheless, the chain of synoptic events after 22 June across the Pacific plays an essential role and additionally limits the predictability of the magnitude of the heat wave. The representation of the heat wave in the ensemble forecasts is thus influenced by a preconditioning of Rossby waves in the West Pacific and limited by synoptic-scale predictability directly prior to the heat wave.

4 Concluding Discussion

In conclusion, our detailed dynamical investigation of the predictability of the Canadian heat wave in June 2021 reveals the dominant role of the downstream development of Rossby waves along the North Pacific jet stream. Diabatic flow amplification due to the outflow of WCB airstreams in establishing the stationary large-scale ridge over Northwest America was essential for the unprecedented heat wave which corroborates results of recent studies (Neal et al., 2022). The chain of synoptic events emerged from unusual precipitation along the Meiyu-Baiu-Front more than 7000 km upstream over the West Pacific and more than 10 days prior to the event. Although the seed of the blocking event may be traced back to the Western Pacific or even to Southeast Asia (Qian et al., 2022; Lin et al., 2022), a successful prediction of the heat wave hinges on the successful prediction of the Eastern Pacific WCB events, and the forecasts initialized before June 22 are not well-conditioned to predict this event accurately. Thus, the complicated scale-interactions involved in the WCB activity, jet amplification, and downstream development constitute a predictability barrier that make accurate forecasts of the heat wave magnitude very unlikely beyond seven days lead time. This contrasts with the fact that the predictability horizon of extremely hot temperatures exceeds the predictability horizon of just above-normal temperature anomalies (Wulff & Domeisen, 2019). The resultant short lead time due to insufficient forecasts in this case may have hampered possible disaster mitigation efforts.

The presence of a predictability barrier due to diabatic processes, in particular WCBs and synoptic activity, was also found for other regions, seasons, and extremes (Sánchez et al., 2020; González-Alemán et al., 2022) and deserves further investigation. The emerging picture that atmospheric dynamical processes on the relatively short synoptic-time scales matter for high-amplitude Rossby waves and states of the jet stream also has implications for understanding the consequences of climate change. It is postulated that stationary high-amplitude Rossby waves become more frequent under climate change (Coumou et al., 2018; Hoskins & Woollings, 2015). In a warmer climate more moisture will be available for latent heat release which may ultimately affect the amplitude of Rossby waves in the way described here. To date, the impact of WCB activity in a future climate is uncertain, in part because of the tug-of-war between potentially increased diabatic heating and concomitant higher isentropic outflow levels of diabatically enhanced weather systems (Joos et al., 2022), and a predicted weakening of dry dynamics/dry synoptic activity (Coumou et al., 2018) through Arctic amplification (Cohen et al., 2014). More work is needed to better understand if WCB activity and synoptic dynamics are accurately represented in climate models and lead to more amplified states of the jet stream in the future.

Acknowledgments

This work was funded by the Helmholtz Association as part of the Young Investigator Group 'Sub-seasonal Predictability: Understanding the Role of Diabatic Outflow' (SPREADOUT, grant VH-NG-1243). The research was partially embedded in the subprojects A8 and B8 of the Transregional Collaborative Research Center SFB/TRR 165 'Waves to Weather' (https://www.wavestoweather.de, last access: 01/2022) funded by the German Research Foundation (DFG). The authors acknowledge support by the state of Baden-Württemberg through bwHPC. ECMWF is acknowledged for granting access to the re-analysis datasets and operational ensemble forecast data.

Figures

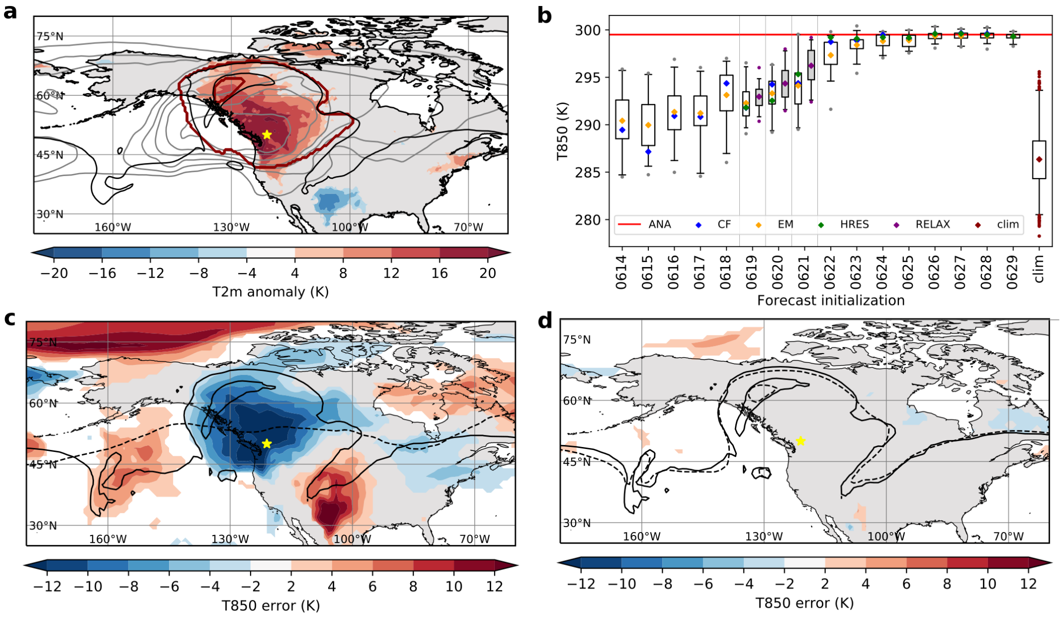

Figure 1. a ERA5 2 m temperature anomaly on 29 June 2021 00 UTC with respect to the June/July ERA5 climatology from 1979–2019 (shading in K). The black line represents the 2 PVU contour on the 335 K isentrope. The red line encloses the upper-level negative PV-anomaly object identified between 500 and 150 hPa, reflecting the upper-level ridge, on 29 June 2021 00 UTC, and the grey contours show frequencies (contour intervals are 2, 10, 20, 30, 40 and 50%) of such negative PV-anomalies between 13 June and 04 July. The yellow star shows the position of Lytton, BC. b Distributions of ensemble forecasts of 850-hPa temperature valid on 29 June 2021 00 UTC averaged between 131° to 111° W and 40° to 60° N (20° x 20° box around Lytton), reflecting the hot air mass, initialised daily at 00 UTC between 14 and 29 June 2021. Colored diamonds represent the control forecast (blue), the ensemble mean (orange) and the high-resolution forecast (green), the box (whiskers) marks the 25-75 inter-quartile (1-99 inter-quantile) range, and the grey dots represent the maximum and minimum values of the ensemble distribution. The grey boxes and purple diamonds represented the ensemble distribution and mean, respectively, of the relaxation experiments initialized on June 19, 20 and 21 (see section 3.3). The red line represents the analyzed (ERA5) 850 hPa temperature. The box (whiskers) located at the label ‘clim’ shows the 25-75 inter-quartile (1-99 inter-quantile) range of the 30-day ERA5 climatology from mid-June to mid-July (15 June to 14 July) between 1979 and 2019, and the dots show values beyond the 1st and 99th percentiles. c Composite-mean 850 hPa temperature errors (shading in K) and 2 PVU contour on 335 K (dashed line) of forecasts in the ‘bad’ category (n=230), and analyzed 2 PVU contour on 335 K (solid line), representing the upper-level ridge, valid on 29 June 00 UTC (see section 2 for a detailed description of the forecast classification). d As c, but for the forecasts classified as ‘good’ (n=230).

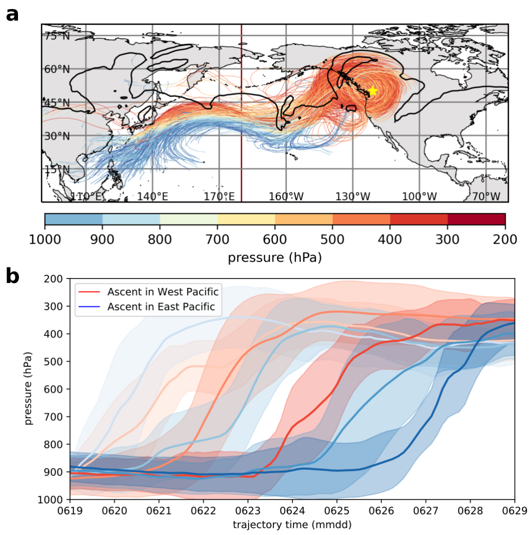

Figure 2. a 10-day backward trajectories initialized within the upper-level ridge over North America on 29 June 00 UTC (see Fig. 1a) which are located below 800 hPa 10 days earlier on 19 June 00 UTC. In total, 20% of all backward trajectories (n=1249) ascend from the lower troposphere into the upper-level ridge. The red line at 180° E marks the separation of the West and East Pacific. b Mean (colored lines) and standard deviation (shading) of the evolution of pressure along the trajectories shown for trajectory clusters separated by their ascent position (red for West Pacific, blue for East Pacific) and the time interval when the ascent occurs. 51% of the trajectories ascend in the West Pacific, 46% in the East Pacific, and 3% of the trajectories are uncategorized.

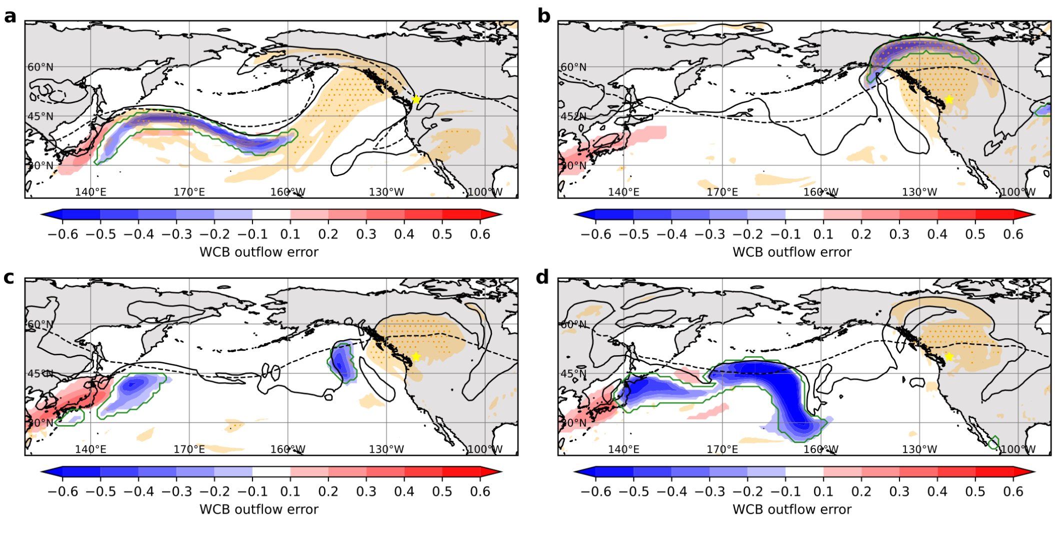

Figure 3. Composite-mean WCB outflow frequency errors (shading) and 2 PVU line on the 335 K isentrope (dashed line) of forecasts classified as 'bad'. The area enclosed by the green line shows WCB outflow in the analysis and the solid black line indicates the analyzed position of the 335 K 2 PVU line. The orange shading (hatching) highlights regions where the tropopause height (i.e. potential temperature on 2 PVU) exceeds the 95th (99th) percentile of the ERA5 dataset (see Supplementary methods in supporting information). Panel a is valid on 24 June, b on 27 June, c on 28 June and d on 29 June.

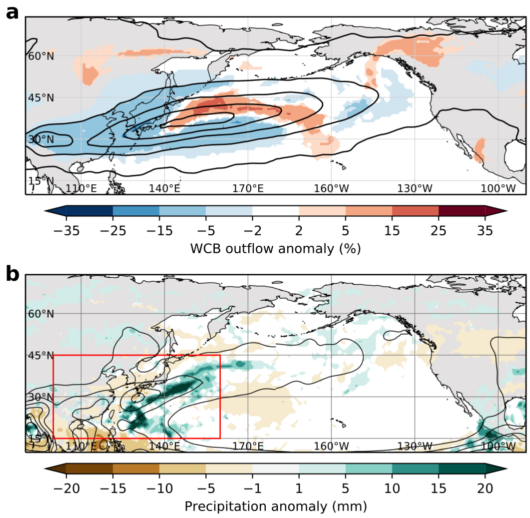

Figure 4. a 15 to 29 June anomalies (shading) and 40-year June ERA5 climatologies (contours) of WCB outflow (contour intervals at 0.5, 5, 10, 15 and 20%). b 15 to 29 June anomalies (shading) and 22-year (2000–2021) climatology of daily GPM IMERG precipitation (Huffman et al., 2019) for June (contour intervals at 3, 6, 9, 12, 15, 18 and 21 mm per day).

Open Research

Data Availability Statement

ERA5 data are freely available at `https://cds.climate.copernicus.eu/cdsapp#!/dataset/10.24381/cds.bd0915c6?tab=overview`. ECMWF ensemble forecast data are available through the TIGGE archive from `https://apps.ecmwf.int/datasets/data/tigge/levtype=sfc/type=cf`. The relaxation experiments will be permanently made accessible through the public KITOpenData repository (https://bwdatadiss.kit.edu/) upon acceptance of this article. Data archiving is currently underway. For the review process, the data can be downloaded from the following repository: `https://bwsyncandshare.kit.edu/s/5CJ26y9ensniiYx`. The relevant data from the relaxation experiments are shown in the Supporting Information Figures S4 and S5. GPM IMERG precipitation data are freely available from `https://doi.org/10.5067/GPM/IMERGDF/DAY/06`.

Code availability

The LAGRANTO documentation and information on how to access the source code are provided in Sprenger and Wernli (2015). Information and the source code for the convolutional neural networks model ELIAS 2.0 are available from Quinting and Grams (2022a), Quinting et al. (2022) and Quinting and Grams (2022b).

References

Abraham, J. (2021). *Record-breaking heat in Canada.* Retrieved Aug 15th 2022, from https://www.rmets.org/metmatters/record-breaking-heat-canada

Bieli, M., Pfahl, S., & Wernli, H. (2015). A lagrangian investigation of hot and cold temperature extremes in europe. *Quarterly Journal of the Royal Meteorological Society*, *141*(686), 98–108. doi: 10.1002/qj.2339

Capuccini, M., & Samenow, J. (2021). *Heat wave blasts U.S. with 150 million Americans under alerts.* Retrieved Aug 15th 2022, from https://www.washingtonpost.com/weather/2021/08/11/heatwave-united-states-pacific-northwest/

Cohen, J., Screen, J. A., Furtado, J. C., Barlow, M., Whittleston, D., Coumou, D., ... Jones, J. (2014). Recent Arctic amplification and extreme mid-latitude weather. *Nature Geoscience*, *7*(9), 627–637. doi: 10.1038/ngeo2234

Coumou, D., Di Capua, G., Vavrus, S., Wang, L., & Wang, S. (2018). The influence of Arctic amplification on mid-latitude summer circulation. *Nature Communications*, *9*(1), 2959. doi: 10.1038/s41467-018-05256-8

Emerton, R., Brimicombe, C., Magnusson, L., Roberts, C., Di Napoli, C., Cloke, H. L., & Pappenberger, F. (2022, aug). Predicting the unprecedented: forecasting the June 2021 Pacific Northwest heatwave. *Weather*, *77*(8), 272–279. Retrieved from https://doi.org/10.1002/wea.4257 doi: https://doi.org/10.1002/wea.4257

Fischer, E. M., Sippel, S., & Knutti, R. (2021). Increasing probability of record-shattering climate extremes. *Nature Climate Change*, *11*(8), 689–695. doi: 10.1038/s41558-021-01092-9

González-Alemán, J. J., Grams, C. M., Ayarzagüena, B., Zurita-Gotor, P., Domeisen, D. I., Gómara, I., ... Vitart, F. (2022). Tropospheric Role in the Predictability of the Surface Impact of the 2018 Sudden Stratospheric Warming Event. *Geophysical Research Letters*, *49*(1), e2021GL095464. doi: 10.1029/2021GL095464

Hauser, S., Teubler, F., Riemer, M., Knippertz, P., & Grams, C. M. (2022). Towards a diagnostic framework unifying different perspectives on blocking dynamics: insight into a major blocking in the North Atlantic-European region. *Wea. Clim. Dyn. Discussions*, *2022*, 1–36. Retrieved from https://wcd.copernicus.org/preprints/wcd-2022-44/ doi: 10.5194/wcd-2022-44

Hersbach, H., Bell, B., Berrisford, P., Hirahara, S., Horányi, A., Muñoz-Sabater, J., ... Thépaut, J. N. (2020). The ERA5 global reanalysis. *Quarterly Journal of the Royal Meteorological Society*, *146*(730), 1999–2049. doi: 10.1002/qj.3803

Hoskins, B. J., McIntyre, M. E., & Robertson, A. W. (1985). On the use and significance of isentropic potential vorticity maps. *Quarterly Journal of the Royal Meteorological Society*, *111*(470), 877–946. doi: 10.1002/qj.49711147002

Hoskins, B. J., & Woollings, T. (2015). Persistent Extratropical Regimes and Climate Extremes. *Current Climate Change Reports*, *1*(3), 115–124. doi: 10.1007/s40641-015-0020-8

Huffman, G., Stocker, E., Bolvin, D., Nelkin, E., & Tan, J. (2019). *GPM IMERG Final Precipitation L3 1 day 0.1 degree x 0.1 degree V06, Edited by Andrey Savtchenko, Greenbelt, MD, Goddard Earth Sciences Data and Information Services Center (GES DISC).* doi: 10.5067/GPM/IMERGDF/DAY/06

Joos, H., Sprenger, M., Binder, H., Beyerle, U., & Wernli, H. (2022). Warm conveyor belts in present-day and future climate simulations. Part I: Climatology and impacts. *Weather and Climate Dynamics Discussions*, *2022*, 1–30. doi: 10.5194/wcd-2022-38

Kornhuber, K., Coumou, D., Vogel, E., Lesk, C., Donges, J. F., Lehmann, J., & Horton, R. M. (2020). Amplified Rossby waves enhance risk of concurrent heatwaves in major breadbasket regions. *Nature Climate Change*, *10*(1), 48–53. doi: 10.1038/s41558-019-0637-z

Lin, H., Mo, R., & Vitart, F. (2022). The 2021 Western North American Heatwave and Its Subseasonal Predictions. *Geophysical Research Letters*, *49*(6), e2021GL097036. doi: 10.1029/2021GL097036

Madonna, E., Wernli, H., Joos, H., & Martius, O. (2014). Warm conveyor belts in the ERA-Interim Dataset (1979-2010). Part I: Climatology and potential vorticity evolution. *Journal of Climate*, *27*(1), 3–26. doi: 10.1175/JCLI-D-12-00720.1

Magnusson, L. (2017). Diagnostic methods for understanding the origin of forecast errors. *Quarterly Journal of the Royal Meteorological Society*, *143*(706), 2129–2142. doi: 10.1002/qj.3072

Mo, R., Lin, H., & Vitart, F. (2022). An anomalous atmospheric river linked to the late June 2021 western North America heatwave. *Research Square*, *in review*. doi: 10.21203/rs.3.rs-1125330/v1

Neal, E., Huang, C. S., & Nakamura, N. (2022). The 2021 Pacific Northwest Heat Wave and Associated Blocking: Meteorology and the Role of an Upstream Cyclone as a Diabatic Source of Wave Activity. *Geophysical Research Letters*, *49*(8), e2021GL097699. doi: 10.1029/2021GL097699

Ninomiya, K., & Shibagaki, Y. (2007). Multi-scale features of the Meiyu-Baiu front and associated precipitation systems. *Journal of the Meteorological Society of Japan*, *85 B*, 103–122. doi: 10.2151/jmsj.85B.103

Petoukhov, V., Petri, S., Rahmstorf, S., Coumou, D., Kornhuber, K., & Schellnhuber, H. J. (2016). Role of quasiresonant planetary wave dynamics in recent boreal spring-to-autumn extreme events. *Proceedings of the National Academy of Sciences of the United States of America*, *113*(25), 6862–6867. doi: 10.1073/pnas.1606300113

Pfahl, S., Schwierz, C., Croci-Maspoli, M., Grams, C. M., & Wernli, H. (2015). Importance of latent heat release in ascending air streams for atmospheric blocking. *Nature Geoscience*, *8*(8), 610–614. doi: 10.1038/ngeo2487

Pfahl, S., & Wernli, H. (2012). Quantifying the relevance of atmospheric blocking for co-located temperature extremes in the Northern Hemisphere on (sub-)daily time scales. *Geophysical Research Letters*, *39*(12). doi: 10.1029/2012GL052261

Philip, S. Y., Kew, S. F., Oldenborgh, G. J. V., Yang, W., Vecchi, G. A., Anslow, F. S., ... Otto, F. E. L. (2021). Rapid attribution analysis of the extraordinary heatwave on the Pacific Coast of the US and Canada June 2021 . *World Weather Attribution*, *2021*(June), 119–123. doi: 10.5194/esd-2021-90

Qian, Y., Hsu, P. C., Yuan, J., Zhu, Z., Wang, H., & Duan, M. (2022). Effects of Subseasonal Variation in the East Asian Monsoon System on the Summertime Heat Wave in Western North America in 2021. *Geophysical Research Letters*, *49*(8), e2021GL097659. doi: 10.1029/2021GL097659

Quinting, J. F., & Grams, C. M. (2022a). EuLerian Identification of ascending AirStreams (ELIAS 2.0) in numerical weather prediction and climate models - Part 1: Development of deep learning model. *Geoscientific Model Development*, *15*(2), 715–730. doi: 10.5194/gmd-15-715-2022

Quinting, J. F., & Grams, C. M. (2022b, aug). *EuLerian Identification of ascending AirStreams (ELIAS 2.0) in numerical weather prediction and climate models - Part 1: Development of deep learning model* (Vol. 15) (No. 2). Zenodo. doi: 10.5194/gmd-15-715-2022

Quinting, J. F., Grams, C. M., Oertel, A., & Pickl, M. (2022). EuLerian Identification of ascending AirStreams (ELIAS 2.0) in numerical weather prediction and climate models - Part 2: Model application to different datasets. *Geoscientific Model Development*, *15*(2), 731–744. doi: 10.5194/gmd-15-731-2022

Quinting, J. F., & Reeder, M. J. (2017). Southeastern Australian heat waves from a trajectory viewpoint. *Monthly Weather Review*, *145*(10), 4109–4125. doi: 10.1175/MWR-D-17-0165.1

Sánchez, C., Methven, J., Gray, S., & Cullen, M. (2020). Linking rapid forecast error growth to diabatic processes. *Quarterly Journal of the Royal Meteorological Society*, *146*(732), 3548–3569. doi: 10.1002/qj.3861

Screen, J. A., & Simmonds, I. (2014). Amplified mid-latitude planetary waves favour particular regional weather extremes. *Nature Climate Change*, *4*(8), 704–709. doi: 10.1038/nclimate2271

Seneviratne, S. I., Zhang, X., Adnan, M., Badi, W., Dereczynski, C., Di Luca, A., ... Zhou, B. (2021). Weather and Climate Extreme Events in a Changing Climate [Book Section]. In V. Masson-Delmotte et al. (Eds.), *Climate change 2021: The physical science basis. contribution of working group i to the sixth assessment report of the intergovernmental panel on climate change* (pp. 1513–1766). Cambridge, United Kingdom and New York, NY, USA: Cambridge University Press. doi: 10.1017/9781009157896.013

Spensberger, C., Madonna, E., Boettcher, M., Grams, C. M., Papritz, L., Quinting, J. F., ... Zschenderlein, P. (2020). Dynamics of concurrent and sequential Central European and Scandinavian heatwaves. *Quarterly Journal of the Royal Meteorological Society*, *146*(732), 2998–3013. doi: 10.1002/qj.3822

Sprenger, M., & Wernli, H. (2015). The LAGRANTO Lagrangian analysis tool - Version 2.0. *Geoscientific Model Development*, *8*(8), 2569–2586. doi: 10.5194/gmd-8-2569-2015

Steinfeld, D., & Pfahl, S. (2019). The role of latent heating in atmospheric blocking dynamics: a global climatology. *Climate Dynamics*, *53*(9-10), 6159–6180. doi: 10.1007/s00382-019-04919-6

Teng, H., Branstator, G., Wang, H., Meehl, G. A., & Washington, W. M. (2013). Probability of US heat waves affected by a subseasonal planetary wave pattern. *Nature Geoscience*, *6*(12), 1056–1061. doi: 10.1038/ngeo1988

Wernli, H., & Davies, H. C. (1997). A Lagrangian-based analysis of extratropical cyclones. I: The method and some applications. *Quarterly Journal of the Royal Meteorological Society*, *123*(538), 467–489. doi: 10.1002/qj.49712353811

White, C. J., Carlsen, H., Robertson, A. W., Klein, R. J., Lazo, J. K., Kumar, A., ... Zebiak, S. E. (2017). Potential applications of subseasonal-to-seasonal (S2S) predictions. *Meteorological Applications*, *24*(3), 315–325. doi: 10.1002/met.1654

Wulff, C. O., & Domeisen, D. I. (2019). Higher Subseasonal Predictability of Extreme Hot European Summer Temperatures as Compared to Average Summers. *Geophysical Research Letters*, *46*(20), 11520–11529. doi: 10.1029/2019GL084314

Yihui, D., & Chan, J. C. (2005). The East Asian summer monsoon: An overview. *Meteorology and Atmospheric Physics*, *89*(1-4), 117–142. doi: 10.1007/s00703-005-0125-z

Zschenderlein, P., Fink, A. H., Pfahl, S., & Wernli, H. (2019). Processes determining heat waves across different European climates. *Quarterly Journal of the Royal Meteorological Society*, *145*(724), 2973–2989. doi: 10.1002/qj.3599

Supporting Information for "Everything hits at once - how remote rainfall matters for the prediction of the Canadian heat 2021"

Oertel, A.[1], Pickl, M.[1], Quinting, J.F., Hauser, S.[1], Wandel, J.[1], Magnusson, L.[2], Balmaseda, M.[2], Vitart, F.[2], Grams, C.M.[1]

[1]Institute of Meteorology and Climate Research (IMK-TRO), Karlsruhe Institute of Technology (KIT), Karlsruhe, Germany

[2]European Centre for Medium-Range Weather Forecasts (ECMWF), Reading, United Kingdom

Contents of this file

This file contains supplementary methods and the supplementary figures S1, S2, S3, S4 and S5.

Corresponding author: A. Oertel, Institute of Meteorology and CLimate Research, Department Troposphere Research (IMK-TRO), Karlsruhe Institute of Meteorology, Wolfgang-Gaede-Strasse 1 76131 Karlsruhe. (annika.oertel@it.edu

Supplementary methods

The relevance of West Pacific heavy precipitation for the process chain leading to the highly amplified upper-level ridge and for the predictability of the event is further underlined using tailored relaxation experiments. Following the approach of Magnusson (2017), the forecast model is nudged towards the analysis in a pre-defined regional box during the model integration, leading to a perfect forecast within the box and reduced forecast errors downstream. Such experiments, comprising 22 ensemble members plus control forecast each, are initialized on 19, 20 and 21 June 00 UTC, with the nudging constrained to the region 100°–160° E, 15°–45° N. For comparison, additional nudging experiments with a box shifted further upstream (60°–100° E, 0°–60° N) were performed.

In the manuscript, the relevance of the rising air airstreams is put into climatological context. The following describes the data sets used for the climatological comparisons. Precipitation anomalies computed from daily precipitation sums retrieved from the Global Precipitation Measurement (GPM IMERG) data set (Huffman et al., 2019) are used to investigate the role of anomalous precipitation over the West Pacific. Data were remapped from their original 0.1° x 0.1° resolution to a coarser resolution of 1.0° x 1.0°. June 2021 precipitation anomalies are computed relative to the June climatology defined over a reduced reference period from 2000 to 2021. To compare the WCB activity prior to the heat wave to the climatological WCB frequency, we calculate 15 to 29 June WCB anomalies with respect to the June climatology from 1979 to 2020. This climatological analysis is based on WCB probabilities computed from ERA5 using ELIAS2.0 (Quinting Grams, 2022a; Quinting et al., 2022; Quinting Grams, 2022b). We also calculate percentiles of tropopause height based on 3-h ERA5 data for the period 1979–2020.

Supplementary figures S1, S2, S3, S4 and S5.

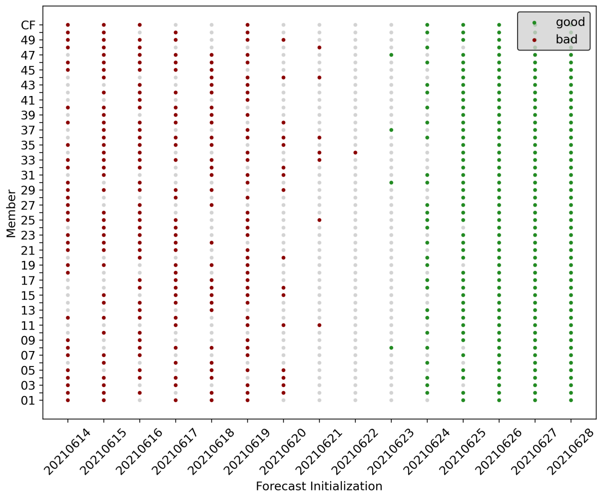

Figure S1. Initialization dates of 'good' (green) and 'bad' (red) forecasts of the medium-range ECMWF ensemble initialised daily at 00 UTC between 14 and 29 June 2021. Both categories comprise 230 forecasts. - Grey dots show neutral forecasts that are neither classified as 'good' nor 'bad' (see Methods for a detailed description of the forecast classification).

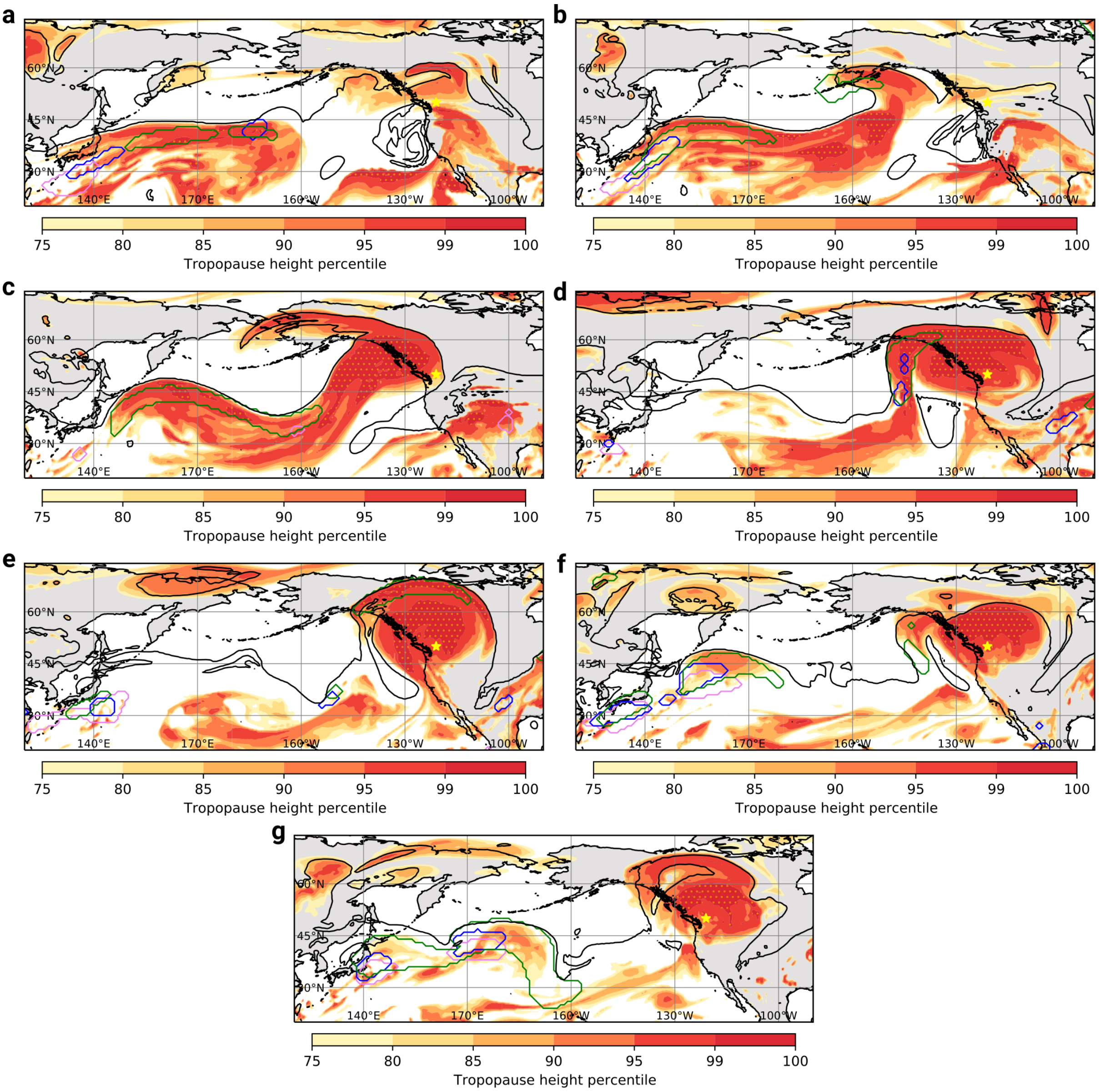

Figure S2. WCB inflow (violet), ascent (blue) and outflow (green contours) and percentiles of tropopause height from ERA5 (shading) for a 22 June 06 UTC, b 23 June 06 UTC, c 24 June 06 UTC, d 26 June 06 UTC, e 27 June 06 UTC, 28 June 06 UTC, g 29 June 00 UTC. Orange hatching highlights regions where the tropopause height (i.e. potential temperature on 2 PVU surface) exceeds the 99th percentile).

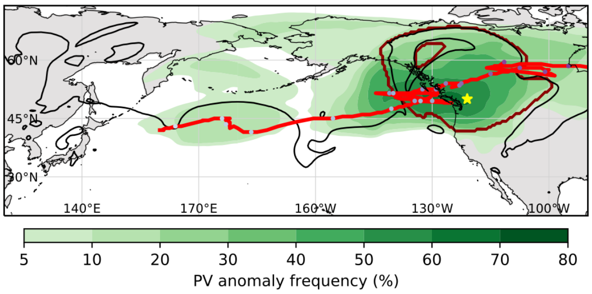

Figure S3. Frequency density of negative upper-level PV anomaly (shading) and the track of its centre of mass (red line) between 13 June and 04 July. The blue dots mark the position every 24 h at 00 UTC and become darker during the time evolution. The upper-level negative PV-anomaly object on 29 2021 00 UTC is outlined in dark red, and the black contour shows the 2 PVU line on 335 K.

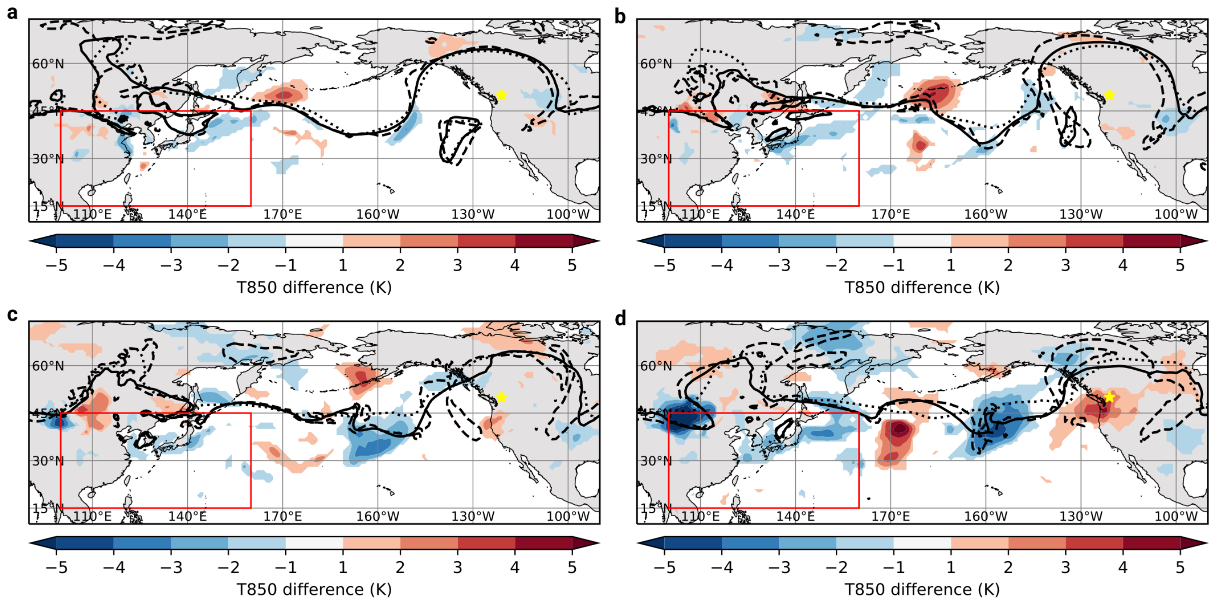

Figure S4. Ensemble-mean temperature differences at 850 hPa between the relaxation and control experiments initialised on 21 June 2021 (shading) and 2 PVU line on 335 K of the relaxation experiment (solid), the control experiment (dotted) and the analysis (dashed), valid on a 26 June 00 UTC, b 27 June 00 UTC, c 28 June 00 UTC, d 29 June 00 UTC. The relaxation domain is depicted by the red box.

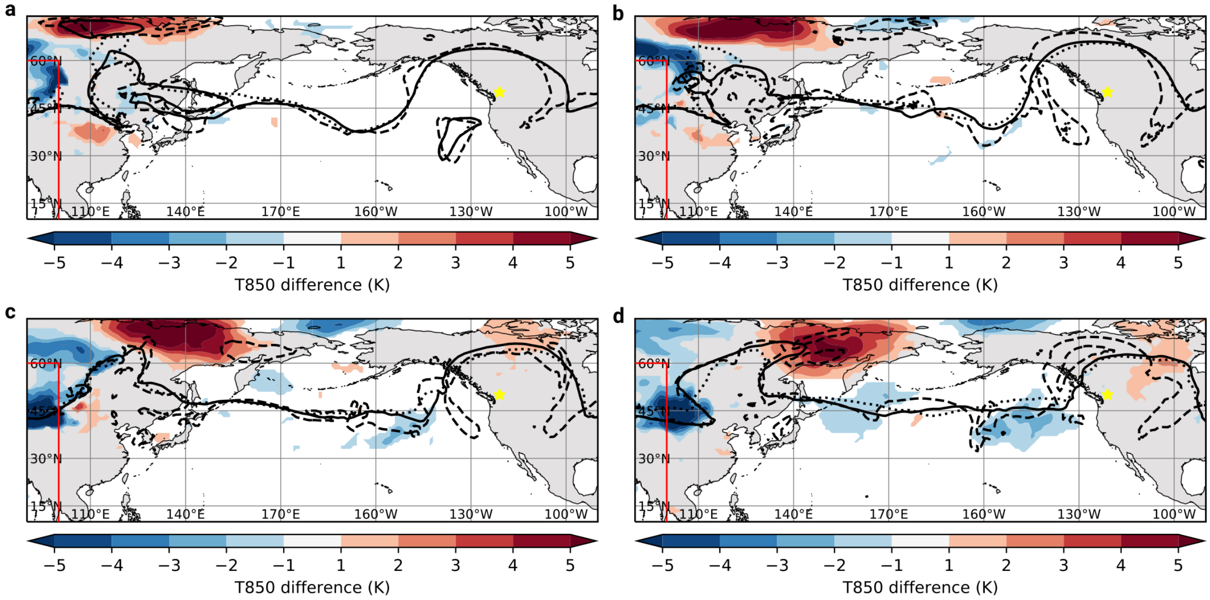

Figure S5. As Figure S4, but for the experiment with the relaxation domain from 60° - 100° E, 0° - 60° N. Note that only the north-western edge of the domain is depicted in the Figure.